Ecological Indicators 102 (2019) 507–518

Contents lists available at ScienceDirect

Ecological Indicators

journal homepage: www.elsevier.com/locate/ecolind

Original Articles

Revegetation has increased ecosystem water-use efficiency during 2000–2014 in the Chinese Loess Plateau: Evidence from satellite data

Han Zheng[a,b], Henry Lin[b,c,*], Weijian Zhou[b], Han Bao[d], Xianjin Zhu[e], Zhao Jin[b,*], Yi Song[b], Yunqiang Wang[b], Wenzhao Liu[f], Yakun Tang[f]

[a] Key Laboratory of Subsurface Hydrology and Ecological Effect in Arid Region of Ministry of Education, School of Environmental Science and Engineering, Chang'an University, Xi'an 710054, China
[b] State Key Laboratory of Loess and Quaternary Geology, CAS Center for Excellence in Quaternary Science and Global Change, Institute of Earth Environment, Chinese Academy of Sciences, Xi'an 710061, China
[c] Department of Ecosystem Science and Management, The Pennsylvania State University, University Park, PA 16802, USA
[d] School of Highway, Chang'an University, Xi'an 710064, China
[e] College of Agronomy, Shenyang Agricultural University, Shenyang 110161, China
[f] State Key Laboratory of Soil Erosion and Dryland Farming on the Loess Plateau, Northwest A&F University, Yangling 712100, China

ARTICLE INFO

Keywords:
Water-use efficiency
Vegetation coverage change
Evapotranspiration
Gross primary productivity
MODIS satellite dataset
Chinese Loess Plateau

ABSTRACT

Vegetation coverage has been effectively increased across the Chinese Loess Plateau (CLP) mainly because of the implementation of large-scale revegetation programs. Understanding the entire CLP's ecosystem carbon-water relationship and its response to the vegetation coverage increase and climate change is essential for the water resources management in this semi-humid to arid region. Water-use efficiency (WUE), defined as the ratio of gross primary productivity (GPP) over evapotranspiration (ET), is an important indicator linking carbon and water cycles at the ecosystem scale. In this study, the spatial and temporal variations in the ecosystem WUE were analyzed to investigate the responses of WUE variation to regional climate and vegetation coverage changes in the CLP using MODerate Resolution Imaging Spectroradiometer (MODIS) datasets of GPP and ET from 2000 to 2014. Results indicate that the spatial pattern of annual WUE was different from that of WUE over active growing season (AGS), generally with higher annual WUE but lower AGS-WUE for the semi-humid southeastern CLP areas. Significant increases were observed in annual and autumn WUE during the study period at both the per-pixel and spatial-average levels, while AGS-WUE, spring WUE, and summer WUE remained quite stable. Correlations between WUE trends and interannual variability of vegetation coverage (expressed as Normalized Difference Vegetation Index or NDVI), precipitation (P), and air temperature (T_a) showed that WUE trends were positively correlated with NDVI variation due to faster increases in GPP as compared to ET caused by enhanced NDVI. Precipitation variation was generally negatively correlated to WUE variation by contributing to faster increases in ET than GPP especially at different seasons. The positive correlations between interannual variability of WUE and T_a were subject to negative feedbacks between ET and T_a. Similar results were also found using net primary productivity (NPP) to calculate ecosystem annual WUE (i.e., NPP/ET). Our findings suggest that revegetation-induced vegetation coverage change rather than P and T_a changes is the primary cause for the increasing ecosystem annual WUE in the CLP. This study contributes to our enhanced understanding of the coupled carbon-water dynamics over regional terrestrial ecosystem under climate and vegetation coverage changes.

1. Introduction

The Chinese Loess Plateau (CLP) is located in the northwest of China with an area of about 640,000 km^2. The CLP is the cradle of ancient Chinese civilization and a critical area implementing the Belt and Road Initiative (Liu, 2015) and the great western development strategy in China (Li et al., 2012). Due to long history of intensified human activities and adverse environmental conditions (e.g., loose loess soils, high precipitation intensity during rainy seasons, and heterogeneous terrain), the CLP is a hot-spot of severe soil erosion and environmental degradation in the world (Feng et al., 2016; Feng et al., 2012; McVicar et al., 2007). To relieve the environmental pressure and to improve the

* Corresponding authors at: Department of Ecosystem Science and Management, The Pennsylvania State University, University Park, PA 16802, USA (H. Lin).
E-mail addresses: henrylin@psu.edu (H. Lin), jinzhao@ieecas.cn (Z. Jin).

https://doi.org/10.1016/j.ecolind.2019.02.049
Received 6 July 2018; Received in revised form 30 January 2019; Accepted 22 February 2019
Available online 08 March 2019
1470-160X/

sustainable development of the CLP, a series of revegetation programs have been carried out since the early 1950s, and remarkable effectiveness in increasing vegetation coverage and reducing soil erosion have been achieved especially after the launch of the Grain for Green (GFG) project (e.g., Chen et al., 2015; Fu et al., 2017). Some concerns about the GFG project and its sustainability have been raised, mainly focusing on the conflicting water demands between vegetation growth and human uses (Chen et al., 2015; Feng et al., 2016). It has been nearly 20 years since the implementation of the GFG project, and it has become urgent to assess to what extent the revegetation has altered the coupled carbon-water dynamics in the CLP terrestrial ecosystems in order to facilitate a more comprehensive understanding of both scientific and policy implications for the water use planning and management in the region.

Ecosystem water-use efficiency (WUE), the ratio of vegetation productivity to ecosystem water loss, is generally defined as the ratio of gross primary productivity (GPP) or net primary productivity (NPP, i.e., GPP minus plant autotrophic respiration) over evapotranspiration (ET) (Hu et al., 2008; Khalifa et al., 2018; Niu et al., 2011; Yu et al., 2004). WUE has been recognized as an important integral indicator linking carbon and water cycles between terrestrial ecosystems and atmosphere, which can help assess ecosystem response to changes in environmental conditions (Huang et al., 2015; Keenan et al., 2013; Niu et al., 2011; Yu et al., 2008). Previous studies have demonstrated that revegetation in the CLP has remarkably influenced the ecosystem carbon and water processes (e.g., Feng et al., 2012; Liu et al., 2014). However, it is still unclear how the vegetation coverage change and climate change affects the trade-off between carbon assimilation and water loss (i.e., WUE) in the CLP, except that Zhang et al. (2016) evaluated the climatic controls on the CLP WUE variations. Despite that the WUE variation and its underlying mechanisms have been well studied at different organismic scales such as plant leaf, plant individual and canopy scales (e.g., Cowan, 1978; Farquhar and Sharkey, 1982; Niu et al., 2011; Yu et al., 2004), it remains challenging to apply the proposed theories (e.g., theories of optimal resource use at leaf level) to evaluate the long-term variation in WUE at larger spatial scales due to the complex interactions between carbon-water processes and vegetation-climatic variability (Niu et al., 2011). Therefore, it is necessary to investigate the spatial and temporal variation in WUE and its responses to regional climate and vegetation coverage changes in the CLP.

Current studies on reginal-scale WUE variations are primarily based on synthesizing site-level observations of vegetation productivity and water loss (Xiao et al., 2013; Zhu et al., 2015). However, upscaling from site-level observations to regional-level remains challenging for WUE studies in the CLP, because of the fragmentized landforms and rare in situ observations in the CLP. Large-scale revegetation makes the site representativeness even more problematic when analyzing the long-term WUE variation in the whole CLP due to temporal changes in ecosystem structures such as species composition and stand age (Fu et al., 2017; Lü et al., 2012). Satellite remote-sensing technology can record large-scale and long-term changes in terrestrial ecosystems with a high spatial-temporal resolution, thus has provided unprecedented datasets for understanding terrestrial water and carbon cycles at the regional and global scales (e.g., Gao et al., 2014b; Yao et al., 2013; Zhang et al., 2010). Incorporating remote-sensing imagery from the MODerate Resolution Imaging Spectroradiometer (MODIS) sensors and gridded meteorological data, MODIS GPP/NPP and ET algorithms were proposed and validated using eddy-covariance flux measurements with good performance (Mu et al., 2011; Running et al., 2004; Zhao et al., 2005). The MODIS global terrestrial GPP/NPP and ET data products (MOD17 and MOD16) obtained since 2000 have been widely applied to various researches on the spatial and temporal variations in terrestrial GPP/NPP, ET, and other related variables (e.g., WUE) at broad spatial scales (e.g., Huang et al., 2017; Sun et al., 2016; Zeng et al., 2014), including the CLP (e.g., Feng et al., 2016; Li et al., 2016; Xiao, 2014; Zhang et al., 2016). Since the GFG project was started almost in sync with the MODIS sensors, it enables us to analyze the long-term variation in the CLP's WUE after implementing the GFG ecological restoration project using continuous satellite-derived data.

Therefore, this study aimed at investigating the spatial and temporal variation in WUE and its responses to regional climate and vegetation coverage changes in the CLP during the time period from 2000 to 2014 mainly based on MODIS GPP/NPP and ET datasets. Three objectivities were proposed: 1) analyzing the spatial patterns of mean annual WUE and mean WUE over active growing season (AGS, i.e., from April to September); 2) evaluating the interannual variability (IAV) of annual WUE, AGS-WUE and WUE values of different seasons (i.e., spring, summer and autumn); 3) exploring the relationships of WUE trends with IAV of remote sensing-based Normalized Difference Vegetation Index (NDVI) as well as ground-based precipitation and air temperature in the CLP.

2. Data and methods

2.1. Study area

The Chinese Loess Plateau (CLP) consists of the entirety or portions of seven administrative divisions in northwestern China (34°-40°N, 102°-114°E, Fig. 1), which comprises approximately 6.7% of the entire land area in China (NDRC et al., 2010). Due to effects of paleogeomorphology and long-term erosion, the landforms in the CLP are basically composed of three typical types: loess tableland (the Yuan), loess ridge (the Liang), and loess hill (the Mao) (Fu et al., 2017; Liu et al., 1978). Loess tablelands mainly distribute in the south of the CLP, while loess ridges and hills generally coexist in the central part of the CLP, i.e., the loess hilly and gully areas in Fig. 1 (NDRC et al., 2010). The loess hilly and gully areas are the hot-spots implementing revegetation schemes including the GFG project (Chen et al., 2015; Feng et al., 2016). The CLP is influenced by a temperate continental monsoon climate and experiences semi-humid, semi-arid, and arid climatic conditions from the southeast to the northwest (Fig. 1). Long-term mean annual temperature of the CLP decreases from lower than 4 °C in the northwest to 14 °C in the southeast, and mean annual precipitation varies from about 200 mm in the northwest to 750 mm in the southeast (Su and Fu, 2013; Xiao, 2014). The CLP is characterized by cold-dry winters and hot-rainy summers, and most precipitation concentrates in the summer rainy season in the form of highly erosive rainstorms (Lü et al., 2012). The vegetation in the CLP is mainly composed of five types of potential natural vegetation, namely forest, forest-steppe, steppe, desert-steppe, and desert (Fig. 1) (Lü et al., 2003).

2.2. MODIS GPP/NPP and ET datasets and WUE calculations

In this study, ecosystem water-use efficiency (WUE) was defined as the ratio of gross primary productivity (GPP) or net primary productivity (NPP) and actual evapotranspiration (ET) (Eq. (1)):

$$\mathrm{WUE} = \frac{GPP}{ET}\left(or\ \mathrm{WUE} = \frac{NPP}{ET}\right) \quad (1)$$

The GPP/NPP and ET estimates were obtained from the MODIS Collection 5 GPP/NPP and ET data products developed by the Numerical Terra Dynamic Simulation Group (MOD17A2/A3 and MOD16A2/A3, http://www.ntsg.umt.edu/, acquired December 20, 2016). The MODIS Collection 5 GPP/NPP algorithm is based on the logic of radiation use efficiency, and calculates annual NPP as the difference between annual GPP and annual autotrophic respiration (including annual growth respiration and annual maintenance respiration by leaves, fine roots and live cells in woody tissue) (Running et al., 2004; Zhao et al., 2005). The MODIS Collection 5 ET algorithm is based on the Penman-Monteith equation (Mu et al., 2007; Mu et al., 2011). The MODIS GPP and ET algorithms showed good performance in generating monthly GPP and ET values of five ecosystems with eddy-

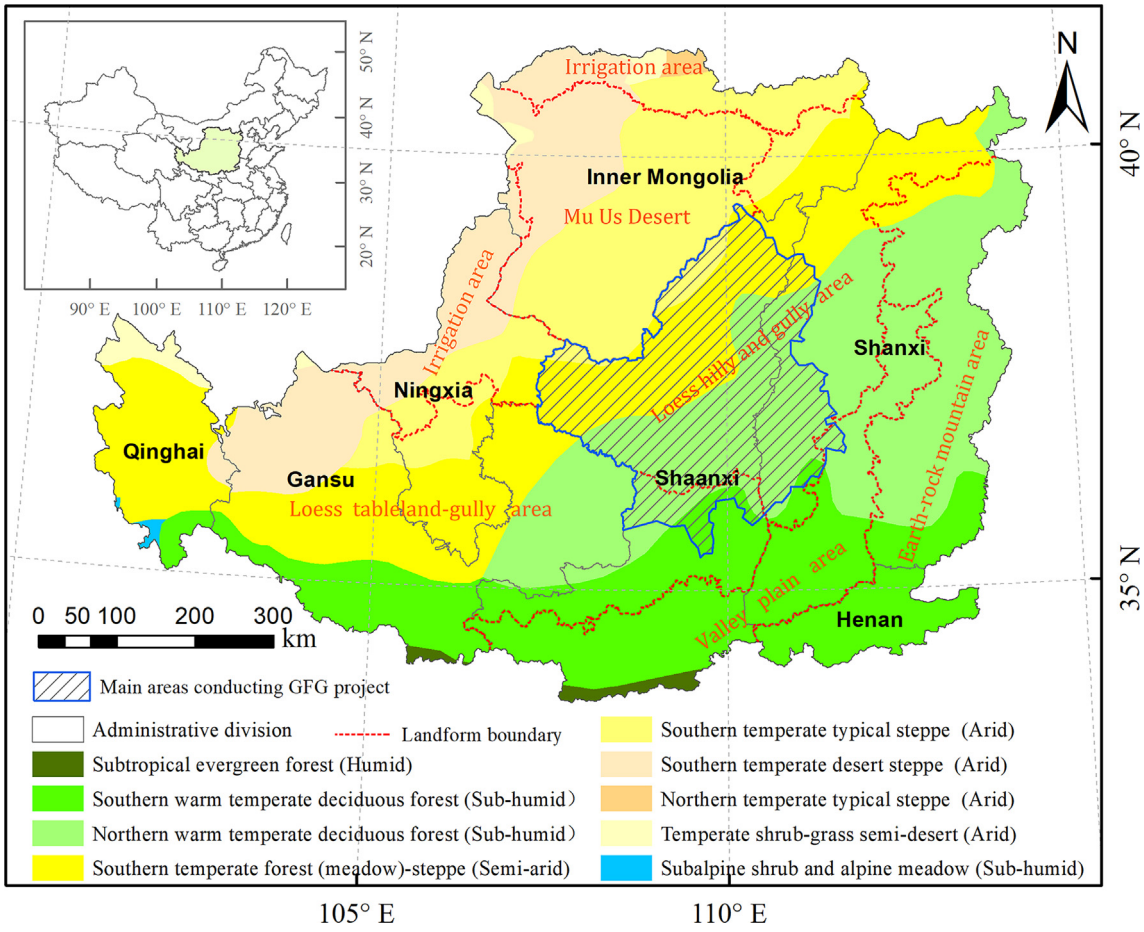

Fig. 1. Location of Chinese Loess Plateau (CLP) and the distribution of typical landforms and potential natural vegetation types. Grey lines show the boundary of seven administrative divisions in the CLP, while the pink dashed lines are the boundary of landforms (NDRC et al., 2010). The blue polygon with slashes shows the main areas with the Grain for Green project implemented (Chen et al., 2015). The color blocks indicate different natural vegetation types (ECVMC, 2007).

covariance GPP and ET measurements in the CLP (Fig. S1). The MODIS Collection 5 GPP/NPP and ET products at monthly and annual time steps and 1 km^2 spatial resolution during the time period 2000–2014 were used in this study.

For the WUE calculations, the annual WUE values (in gC $kg^{-1}H_2O$) were calculated as the ratio of annual GPP (i.e., the sum of GPP values during each year with a unit of gC m^{-2} $year^{-1}$) over annual ET (i.e., the sum of ET values during each year with a unit of mm $year^{-1}$ or kgH_2O m^{-2} $year^{-1}$) for each 1 km^2 pixel during 2000–2014. Annual NPP was also utilized to calculate ecosystem annual WUE (i.e., WUE_{NPP} = NPP/ET) in this study. The monthly composites of GPP and ET data from April to September were aggregated to calculate the GPP and ET over the active growing season (AGS) and then AGS-WUE (i.e., the ratio of AGS-GPP to AGS-ET) in each year at the grid-cell scale. WUE values of different seasons, i.e., spring (from March to May), summer (from June to August), autumn (from September to November), and winter (from December to February), were also calculated for each year over the study period. Grid cells missing GPP/NPP or ET values were masked from the specific WUE datasets.

2.3. NDVI and meteorological datasets

To compare the responses of WUE variation to changes in vegetation coverage and climatic conditions in the CLP, the relationships of WUE variation with NDVI, precipitation (P) and air temperature (T_a) were analyzed in this study. NDVI is an important proxy for vegetation canopy greenness and structure, which is derived from spectral reflectance in the red and near-infrared wavebands (Zhu et al., 2013). We obtained NDVI data at monthly intervals and 1 km^2 spatial resolution during 2000–2014 from a MODIS data product (MOD13A3, https://ladsweb.modaps.eosdis.nasa.gov/, acquired June 29, 2017).

The monthly gridded datasets of P and T_a were generated by the equivalent observed meteorological data at about 756 national basic meteorological stations in China acquired from the China Meteorological Data Service Center (http://data.cma.cn/, acquired June 23, 2017). We first obtained their monthly gridded datasets across the entire China region at the 1 km^2 spatial resolution during 2000–2014 using the method of thin-plate smoothing splines in AUSPLIN software (Hutchinson, 1995; Zheng et al., 2016), which takes a digital elevation model (DEM) as a third independent variable. Then, the monthly gridded datasets for each meteorological variable over the CLP region were extracted from the corresponding gridded datasets during the study period.

Based on the monthly gridded datasets of NDVI and T_a acquired above, the 12 monthly composites for each variable were averaged to calculate the corresponding annual values in each year for each 1 km^2 grid-cell, respectively. As to P, the 12 monthly composites were summed to calculate annual P in each year at the grid-cell scale. AGS and seasonal values for NDVI, P and T_a were also calculated.

2.4. Data analysis

The spatial patterns of annual WUE, GPP and ET in the CLP were analyzed by averaging the annual WUE, GPP and ET data across the 15 years (i.e., 2000–2014) on a per gridded-cell basis, respectively. Grid cells with mean annual NDVI (from MODIS MOD13 dataset) lower than

0.1 were masked in the spatial and subsequent temporal analyses (Zhu et al., 2013). The spatial patterns of AGS-based WUE, GPP and ET during 2000–2014 were also analyzed. We also calculated the latitudinal and longitudinal patterns of WUE by averaging the WUE values of gridded-cells in the same rows and columns, respectively.

To assess the temporal variation in WUE, we calculated the linear trends (i.e., the slope values) of per-pixel annual WUE during 2000–2014 using the method of ordinary least square regression of annual WUE vs. year. Grid-cell series with missing values during the study period were discarded. The per-pixel temporal trends were considered to be significant if *p*-values are smaller than 0.05. Apart from spatial patterns of annual WUE trends, we also examined the linear regression slope of annual WUE at the spatial-average level (i.e., all the pixels in the CLP were averaged) during 2000–2014. The linear trends were also examined for the AGS-WUE and WUE values of different seasons at both the per-pixel and spatial-average levels. The linear trends of GPP, ET, NDVI, *P* and T_a were also analyzed for annual, AGS and different seasons.

Pearson's correlation analyses were performed for each pixel to investigate the relationships of WUE trends with NDVI, *P* and T_a trends. To avoid spurious correlation between two variables caused by their same varying direction, the time series were detrended prior to the correlation analysis (Xiao, 2014). The correlations of AGS and seasonal series of WUE with equivalent series of GPP, ET, NDVI, *P* and T_a were also analyzed on the per gridded-cell basis.

3. Results

3.1. Spatial patterns of WUE in the CLP

Distinct spatial variations were observed for the per-pixel mean annual WUE and mean AGS-WUE during 2000–2014 (Fig. 2). The mean annual WUE was generally lower in the arid and semi-arid areas, and higher in the more humid areas where water was more available (naturally or due to irrigation), with the per-pixel mean annual WUE ranging from 0.06 to 3.26 g C kg^{-1} H_2O and the overall spatial average of 1.26 ± 0.28 g C kg^{-1} H_2O (Fig. 2a and Table 1). The mean AGS-WUE tended to be higher in the less humid northwestern CLP and the irrigation areas (Fig. 1), and lower in the more humid areas, with per-pixel mean AGS-WUE values varying between 0.09 and 6.16 g C kg^{-1} H_2O and the overall spatial average of 2.09 ± 0.47 g C kg^{-1} H_2O (Fig. 2b and Table 1).

The differences in the spatial patterns of annual WUE vs. AGS-WUE were also observed within their latitudinal and longitudinal mean patterns (Fig. 2, left and bottom panels). The latitudinal mean annual WUE during 2000–2014 tended to increase with the decrease in latitude (Fig. 2a, left panel), while the latitudinal mean AGS-WUE significantly declined with the decrease in latitude (Fig. 2b, left panel).

3.2. Temporal variations of WUE in the CLP

Spatial variations in the CLP WUE trends derived from MODIS datasets are shown in Fig. 3. Results indicated that annual WUE significantly increased over 68.9% of the entire CLP area from 2000 to 2014 (*p*-value < 0.05, Table 2), with much higher increases in the loess hilly and gully areas (Fig. 3a1). For these areas with significant positive trends, 60% were caused by mutual increases in annual GPP and annual ET but with faster increases in annual GPP, and 36.4% were induced by positive GPP and negative ET trends (Fig. 3b1, and Fig. S2). The area showing a significant decrease in annual WUE only occupied 0.3% of the entire CLP region (Table 2).

The spatial variations in the AGS-WUE trends during 2000–2014 showed significant increases across 23.1% of the CLP area (Table 1); of these, 68.3% were led to by positive trends in both the AGS-GPP and AGS-ET rates (Fig. 3a2 and b2). Significant decreases in the AGS-WUE occurred over 4.6% of the entire region (Table 2), mainly due to asymmetric increases in AGS-GPP and AGS-ET with faster increases in AGS-ET (Fig. 3a2 and b2). Table 2 also shows that spring WUE and summer WUE remain quite stable over most areas in the CLP during the study period. In contrast, autumn WUE significantly increased over 58% of the entire CLP area during 2000–2014 (Fig. 3a5 and Table 2); of these, 75.3% were attributed to increasing autumn GPP and decreasing autumn ET (Fig. 3b5).

For the overall spatial-average level (i.e., all the pixels in the CLP were averaged), a significant increase has been observed in the annual WUE and autumn WUE during 2000–2014, with an increase of 0.02 and 0.03 gC $kg^{-1}H_2O$ yr^{-1}, respectively (*p*-value < 0.05, Figs. 4 and 5). WUE of AGS, spring, summer and winter remained stable with no significant change, although pronounced increases in AGS and summer GPP and ET values were manifested (Figs. 4 and 5).

During the study period, per-pixel annual NDVI significantly increased over 81% of the CLP area, with higher increasing trends mainly distributed in the loess hilly and gully areas (Fig. S3a1). Similar patterns for the NDVI trends were also observed for the AGS and different seasons (Fig. S3a). Per-pixel precipitation (*P*) also increased over most areas in the CLP at different seasons (except winter), but the trends were substantially non-significant (Fig. S3b). The per-pixel mean annual air temperature (T_a) decreased in most areas but with significant decreasing trends over about 1% of the entire CLP region (Fig. S3c). Our results also indicated significant increasing trends in NDVI values (*p*-value < 0.001) but non-significant trends in *P* and T_a during 2000–2014 at the spatial-average level (Figs. 4b and 5b).

3.3. Relationships of WUE trends with NDVI, precipitation and temperature trends

Fig. 6a provides the spatial patterns of correlation coefficients (*R*) between detrended IAV of WUE and NDVI. Results showed that IAV of annual WUE was positively correlated with IAV of annual NDVI around 82% of the CLP region, with *R* values larger than 0.5 over 34.8% of these positive areas (Fig. 6a1). Similar spatial distributions of correlations were found between the IAV of autumn WUE and autumn NDVI, where positive correlations occurred in 66.4% of the CLP area but with consistently lower *R* values as compared to annual timeframe ($R > 0.5$ in 9.7% of the CLP area, Fig. 6a5). Negative correlations between IAV of WUE and NDVI were observed across 71.1% and 75% of the entire CLP region for the AGS and summer, with strong correlations ($R < -0.5$) occurred over 21% and 28.8% of these areas, respectively (Fig. 6a2 and a4).

Per-pixel correlations between IAV of WUE and *P* showed negative *R* values over most areas in the CLP during 2000–2014 (Fig. 6b). About 72% of the CLP area showed negative correlations between detrended IAV of annual WUE and annual *P*, with strong correlations ($R < -0.5$) over 19.3% of these negative pixels (Fig. 6b1). For the autumn, IAV of autumn WUE was strongly and negatively correlated with that of autumn *P* over more than 50% of the CLP area during the study period (Fig. 6b5).

Fig. 6c shows similar spatial patterns of the correlations between WUE and T_a for annual, AGS and different seasons, always with positive *R* values for most CLP areas. Positive correlations between annual WUE and T_a were found in 83.5% of the CLP area, with strong correlations over 10% of these positive pixels (Fig. 6c1).

4. Discussion

4.1. Spatial variations in annual WUE and AGS WUE in the CLP

Ecosystem WUE is an important ecological indicator reflecting the water constrains on the vegetation productivity and carbon sequestration capacity (Beer et al., 2009; Zhu et al., 2015). Defined as the ratio of GPP to ET, spatial patterns of ecosystem WUE are regulated by both the carbon assimilation and water loss processes (Sun et al., 2016). In this

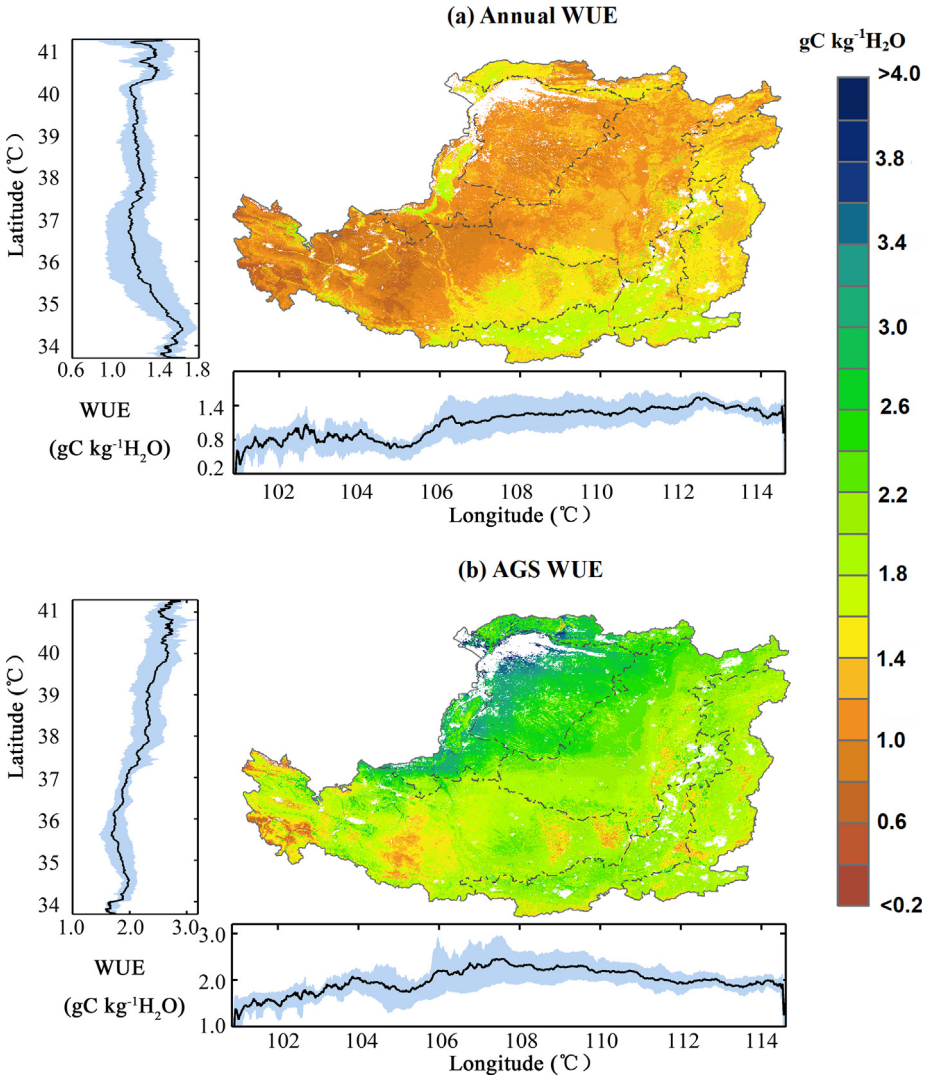

Fig. 2. Spatial patterns of (a) annual WUE and (b) active growing season (AGS) WUE in the CLP averaged from 2000 to 2014. The left and bottom insets show the latitudinal and longitudinal patterns of WUE, respectively. Black lines and shaded areas in insets refer to the mean WUE values and the intervals between the first and third quartiles of WUE ensemble along the latitude or longitude gradients, respectively. Grey dashed lines inside the maps show the boundary of typical landforms as shown in Fig. 1.

study, the spatial distributions of GPP and ET in the CLP derived from MODIS products were similar in terms of both mean annual and AGS values during 2000–2014, consistently showing higher values in the more humid and warmer southeastern areas (Fig. S4). However, the differences in the magnitudes of GPP and ET led to the spatial gradients in WUE, as well as distinct spatial patterns of annual and AGS WUE (Fig. 2).

Although the spatial patterns of WUE (both annual and AGS) were changing during 2000–2014 under the effects of vegetation coverage and climate changes as discussed below, there are no essential differences in the spatial distributions of WUE (Figs. S5–S6). The mean annual WUE values were generally higher in areas with relatively more water supply (i.e., forest and irrigation areas) (Fig. 2a), which agree with the global and CLP-regional patterns of mean annual WUE reported in previous studies (Sun et al., 2016; Zhang et al., 2010). The positive tendency of mean annual WUE along precipitation gradients has also been confirmed by synthesizing real-world ecosystem-scale eddy covariance measurements in China (Xiao et al., 2013; Zhu et al.,

Table 1
Mean annual WUE and mean AGS-WUE estimates (gC kg^{-1} H_2O) for different landform zones in the CLP during 2000–2014. The ratios of annual GPP and annual ET distributed in the AGS are also provided.

Landform zone	Annual WUE	AGS-WUE	AGS-GPP/Annual GPP	AGS-ET/Annual ET
Valley plain area	1.60 ± 0.19	1.97 ± 0.26	0.85 ± 0.04	0.69 ± 0.05
Earth-rock mountain area	1.45 ± 0.17	1.88 ± 0.23	0.88 ± 0.05	0.68 ± 0.06
Loess tableland-gully area	1.14 ± 0.31	1.79 ± 0.35	0.91 ± 0.04	0.59 ± 0.10
Loess hilly and gully area	1.24 ± 0.17	2.12 ± 0.28	0.91 ± 0.03	0.54 ± 0.09
Irrigation area	1.26 ± 0.28	2.61 ± 0.41	0.91 ± 0.03	0.46 ± 0.12
Mu Us Desert area	1.15 ± 0.15	2.78 ± 0.38	0.90 ± 0.03	0.38 ± 0.06
CLP mean	1.26 ± 0.28	2.09 ± 0.47	0.90 ± 0.04	0.56 ± 0.13

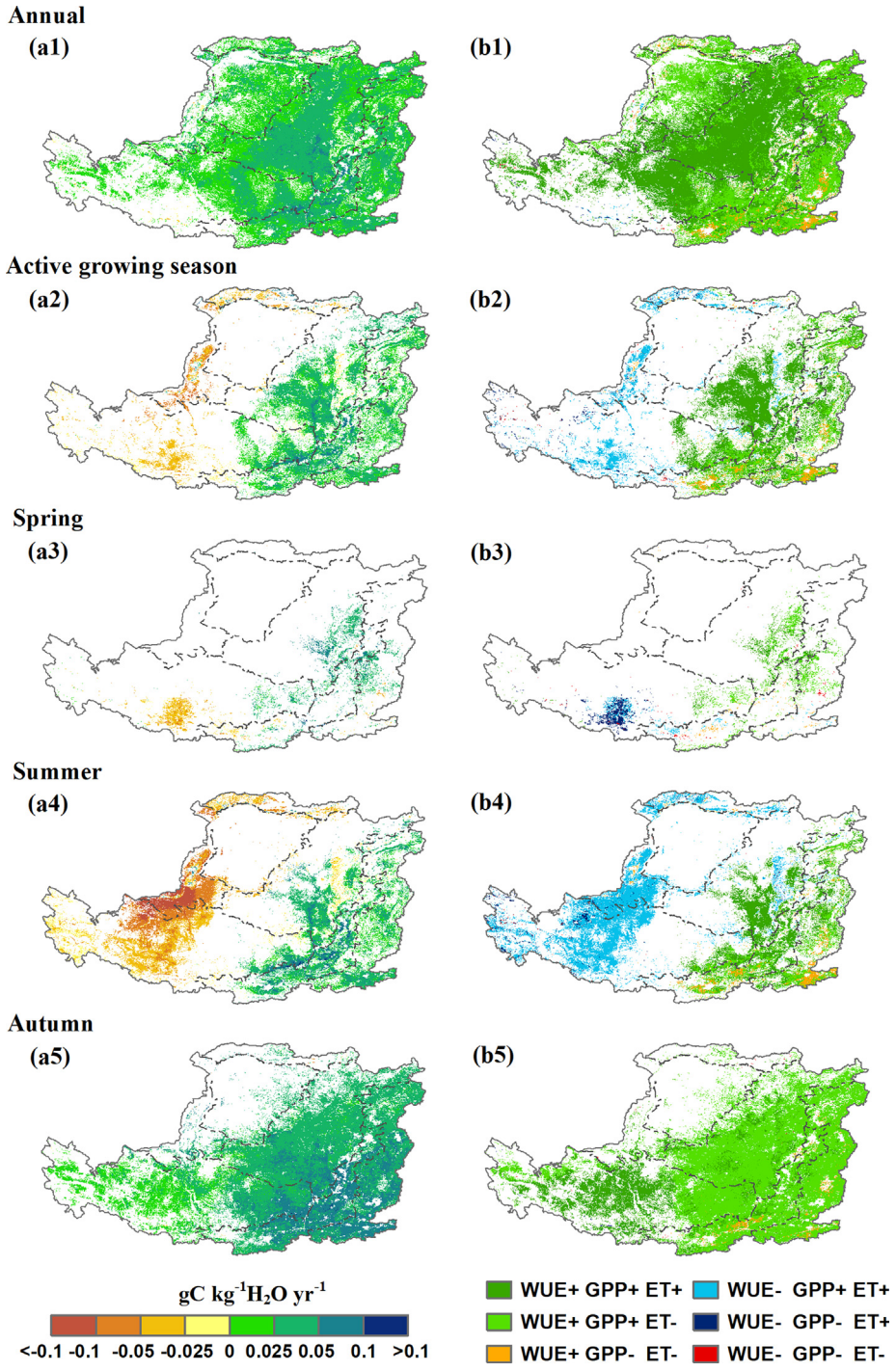

Fig. 3. Spatial patterns of (a) WUE trends and (b) composite maps of the sign of WUE, GPP and ET trends during 2000–2014 at the timeframes of (1) annual, (2) active growing season, (3) spring, (4) summer, and (5) autumn in the CLP. In the legend of Panels (b), the symbol '+' represents positive trend, and '−' refers to negative trend during the study period. Only WUE trends at the significant level p-value < 0.05 are shown in the figures.

2015). It is because that, the forest vegetation in the more humid areas generally has denser canopies and higher root surfaces, which could intercept more solar radiation and utilize more soil, and hence benefit the plant growth and ecosystem WUE (Hu et al., 2008; Niu et al., 2011). For the irrigated areas, the higher WUE was also contributed by the higher dry matters (i.e., higher GPP) yielded by cultivated cropland, which are usually fertilized, in the irrigation areas (Zhang et al., 2010).

The spatial dependence of annual WUE on water availability in the CLP could also be explained by the complicated water loss processes at the ecosystem scale (Niu et al., 2011; Sun et al., 2016; Zhu et al., 2015). Ecosystem ET is generally divided into plant transpiration (T) and evaporation from soil and canopy interception (E) (Wang and Dickinson, 2012; Zheng et al., 2016), which makes ecosystem WUE as the product of GPP/T (i.e., plant WUE) and T/ET. GPP/T is mainly affected by the adaption of plants to the environment, which has a much weaker dependence on precipitation than ecosystem WUE (i.e., GPP/ET) (Sun et al., 2016). T/ET reflects the water allocation between physical and biological processes, varying with vegetation coverage and climatic conditions (Hu et al., 2008; Law et al., 2002). Previous observation and modeling results indicated that higher rates of water

Table 2
Proportions of areas showing significant increasing and decreasing trends (p-value < 0.05) in WUE, GPP and ET, and WUE trends at the spatial-average level for annual, AGS and different seasons in the CLP during 2000–2014.

	WUE		GPP		ET		Spatial-average WUE trend
	Increase	Decrease	Increase	Decrease	Increase	Decrease	Slope(p-value)
Annual	68.9%	0.3%	64.8%	0.9%	18.0%	6.6%	0.02 (< 0.001)
AGS	23.1%	4.6%	60.6%	0.9%	41.1%	2.1%	0.003 (0.70)
Spring	3.7%	1.5%	33.8%	2.8%	2.8%	1.4%	0.01 (0.66)
Summer	15.8%	15.0%	54.6%	0.8%	46.7%	2.1%	−0.004 (0.67)
Autumn	58.1%	0.1%	63.6%	0.7%	2.3%	6.2%	0.03 (< 0.01)

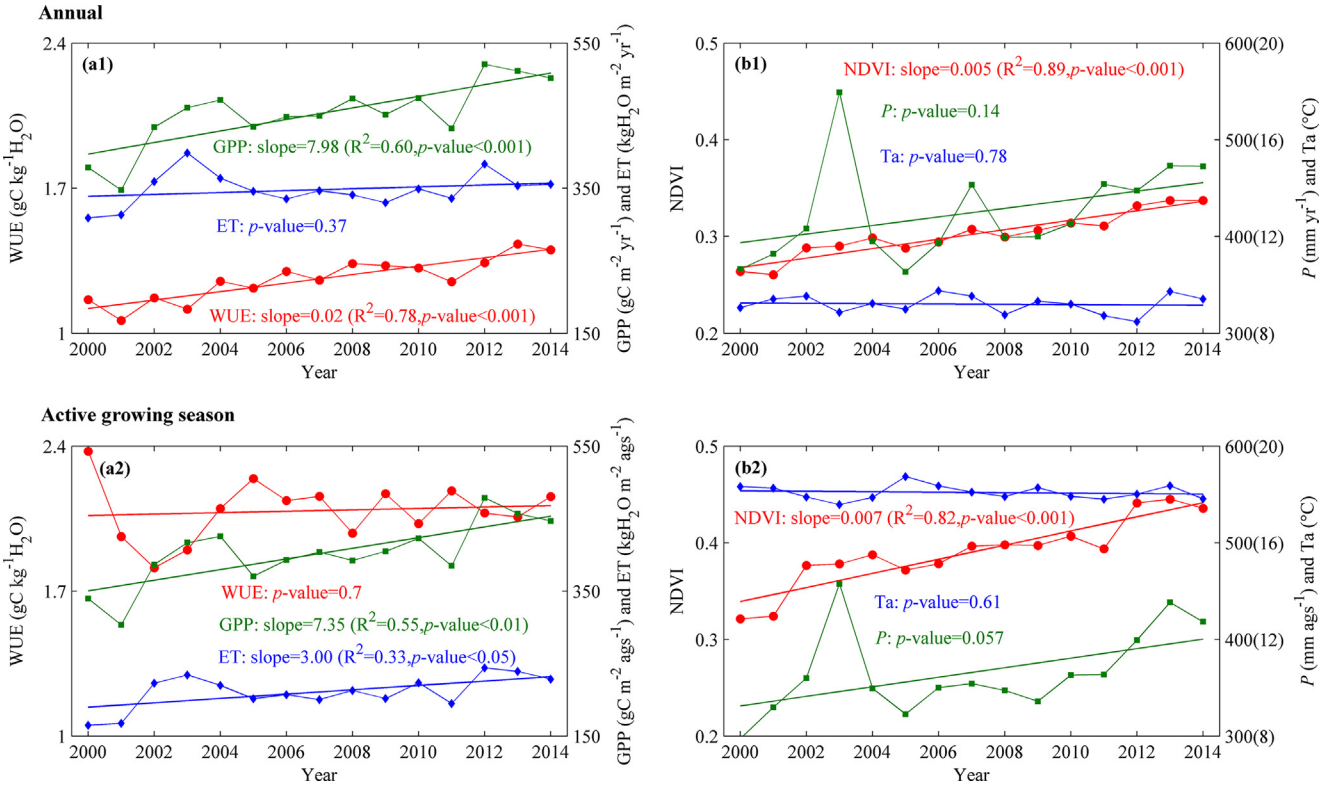

Fig. 4. Interannual variability of (a1) annual and (a2) AGS-based WUE, GPP and ET across the CLP at the spatial-average level during 2000–2014. The IAV of (b1) annual and (b2) AGS-based NDVI, P, and T_a are also shown for reference. The values in the brackets of right y-axis labels in Panels (b) are for T_a.

supply and warmer climate act to increase vegetation coverage and T/ET (Hu et al., 2008; Jasechko et al., 2013; Zheng et al., 2016), thereby increasing WUE. Based on this, the contribution of T to ET for the humid, sub-humid and irrigation areas in the CLP should be larger as compared to the arid and semi-arid areas with sparse vegetation coverage and low humidity (e.g., Mu Us Desert areas in the CLP), leading to the corresponding spatial differences in the mean annual WUE among different climatic zones in the CLP. It has also been reported that high altitudes could limit plant growth (i.e., GPP) and lead to decreases in T/ET and WUE because of corresponding low CO_2 partial pressure and air temperature (Gao et al., 2014a; Zhu et al., 2015). This might contribute to the lowest mean annual WUE values observed in the central and western parts of loess tableland-gully areas, in consideration of their much higher altitudes (> 2000 m) than other areas of the CLP (Su and Fu, 2013).

Compared to the mean annual WUE in the CLP, the mean AGS-WUE showed higher values but quite distinct spatial patterns, particularly exhibiting an almost opposite latitudinal distribution to that of the mean annual WUE (Fig. 2, left panels). The mean AGS-WUE values were much higher for the relatively drier areas in the northwestern CLP (e.g., Mu Us Desert areas), but tended to be lower for the more humid areas in the southeastern CLP (Fig. 2b). This could be explained by the different seasonal distributions of GPP and ET responding to precipitation gradients. Note that the ratio of AGS-ET to annual ET (i.e., AGS-ET/annual ET) in the CLP showed obvious decreasing trend from southeastern to northwestern CLP areas on average, with much lower AGS-ET rates (accounting < 50% of annual ET) in the arid and sub-arid ecosystems (Fig. S4c2 and Table 1). On the contrary, about 90% of annual GPP uniformly occurred during AGS in the CLP (Fig. S4c1). It indicates that the limited water supply under warmer temperatures in the less humid areas could reduce ecosystem water loss more seriously than vegetation productivity, especially that water stress reduces plant transpiration per unit of GPP due to stomatal regulation (Farquhar and Sharkey, 1982; Niu et al., 2011), thereby leading to higher mean AGS-WUE for the drier northwestern CLP region.

4.2. Responses of CLP WUE trends to vegetation coverage and climate changes

Previous studies have concluded that the responses of WUE to various factors (e.g., vegetation coverage, P and T_a) depend on the dominant processes driving plant photosynthesis and ecosystem water loss, and the resulted relative changes in GPP as compared to ET (Huang et al., 2015; Niu et al., 2011; Zhu et al., 2011). In this study,

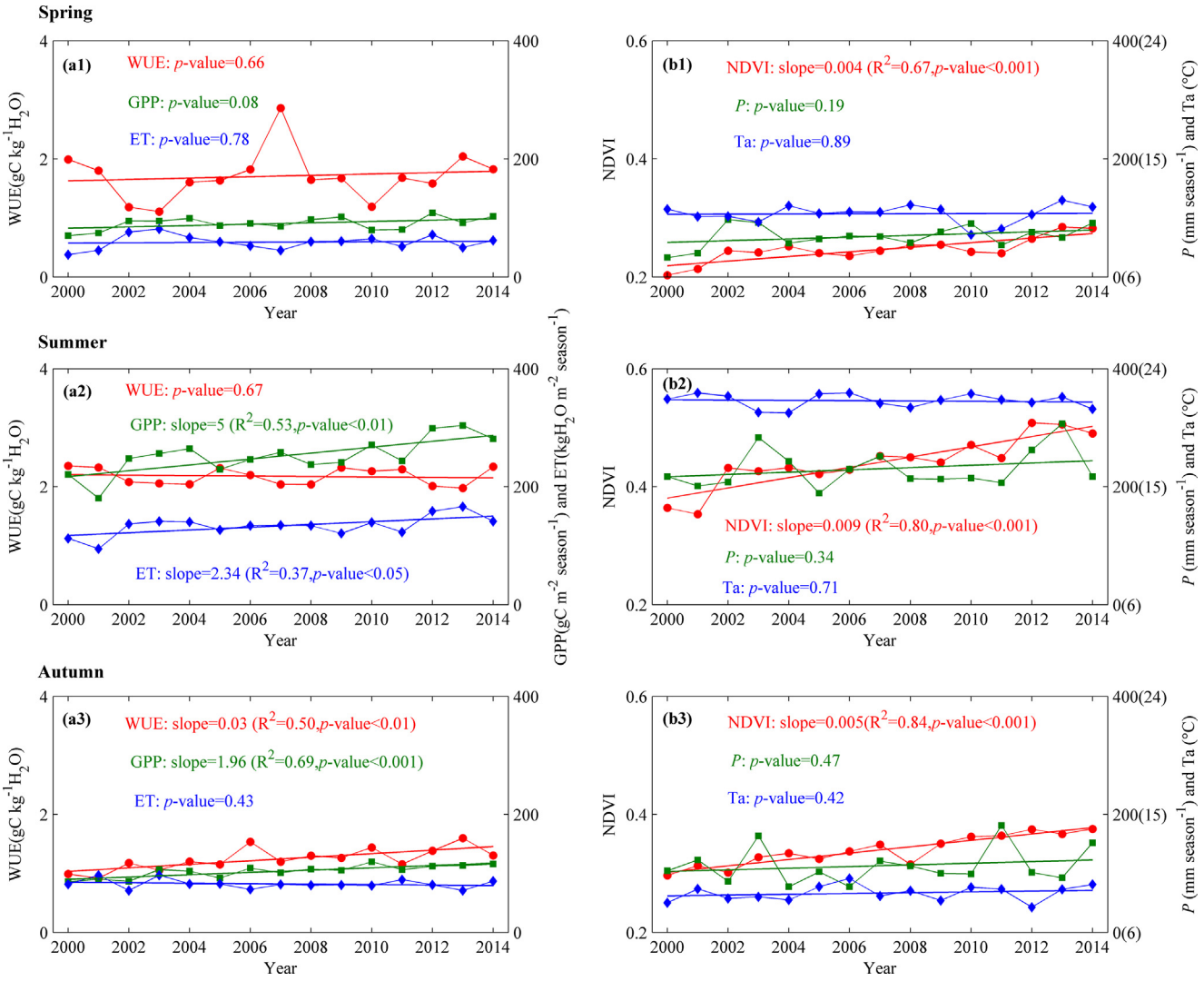

Fig. 5. Interannual variability of WUE, GPP, and ET (a1) spring, (a2) summer and (a3) autumn at the spatial-average level in the CLP during 2000–2014. The IAV of (b1) spring, (b2) summer and (b3) autumn NDVI, *P*, and T_a are also shown for reference. The values in the brackets of right *y*-axis labels in Panels (b) are for T_a.

GPP and ET derived from MODIS products were both significantly enhanced with increased NDVI in most situations (with positive *R* values), but the increasement of GPP exceeded ET (with higher *R* values) (Panels a in Figs. 7 and 8). Accordingly, positive responses of WUE to NDVI should be produced. The increased vegetation coverage at high NDVI is expected to increase the plant transpiration and evaporation of canopy interception (Jung et al., 2011; Piao et al., 2007), but reduce the soil evaporation at the same time (Hu et al., 2008; Law et al., 2002) with declining fraction of solar radiation reaching the soil surface (Beer et al., 2009). Law et al. (2002) found that the proportion of total ET evaporated from soil surfaces decreased from more than 30% to zero as LAI increased from 0.5 to about 2.5 for the forest ecosystems with different climate conditions. Thus, the downregulated ET from reduced soil evaporation may to some extent offset the increase in ET from increased NDVI, hence leading to an increase of WUE. Moreover, increase in the ratio of plant transpiration to ecosystem ET (i.e., T/ET) may also contribute to the increasing WUE at higher NDVI. In addition, the decreased runoff due to revegetation and slightly changed precipitation in the CLP (Feng et al., 2012; Li et al., 2016) could reduce nitrogen loss (Yu et al., 2017), leading to an improvement in soil nutritional status and plant growth, and thus enhancing GPP and then WUE.

The IAV of GPP and ET both positively responded to increasing *P* in most parts of the CLP at different timeframes (i.e., annual, AGS and different seasons) during the study period, and increasing *P* stimulated ET more than GPP (with higher *R* values) (Panels b in Figs. 7 and 8) and eventually lead to negative correlations between changes of WUE and *P* (Fig. 6b). On one hand, the increasing cloudy days from increasing precipitation events especially in summers may cause some limitation for plant growth additionally with cold winter temperature (Nemani et al., 2003). On the other hand, high-intensity precipitation in the CLP (Fu et al., 2017) usually causes ineffective water use associated with plant growth (Huxman et al., 2004; Niu et al., 2011). Therefore, increasing *P* has a stronger positive correlation with ET as compared to GPP, and is expected to decrease WUE as a result. Contrary to *P*, changes of ET were negatively correlated with T_a across most CLP areas for all the timeframes discussed, while the correlations between GPP and T_a varied but with lower negative correlations as compared to ET (Panels c in Figs. 7 and 8), hence producing positive impacts on WUE (Fig. 6c). This is mainly due to negative feedbacks between ET and T_a, that the enhanced ET resulting from revegetation could exert cooling effects on the climate by increasing latent heat flux in the CLP (Xiao, 2014).

4.3. Dominant factors driving temporal variations in the CLP WUE

Against the background of revegetation schemes and climatic fluctuations, the spatial patterns of ecosystem-level WUE trends in the CLP derived from MODIS datasets varied at different timeframes (Fig. 3a).

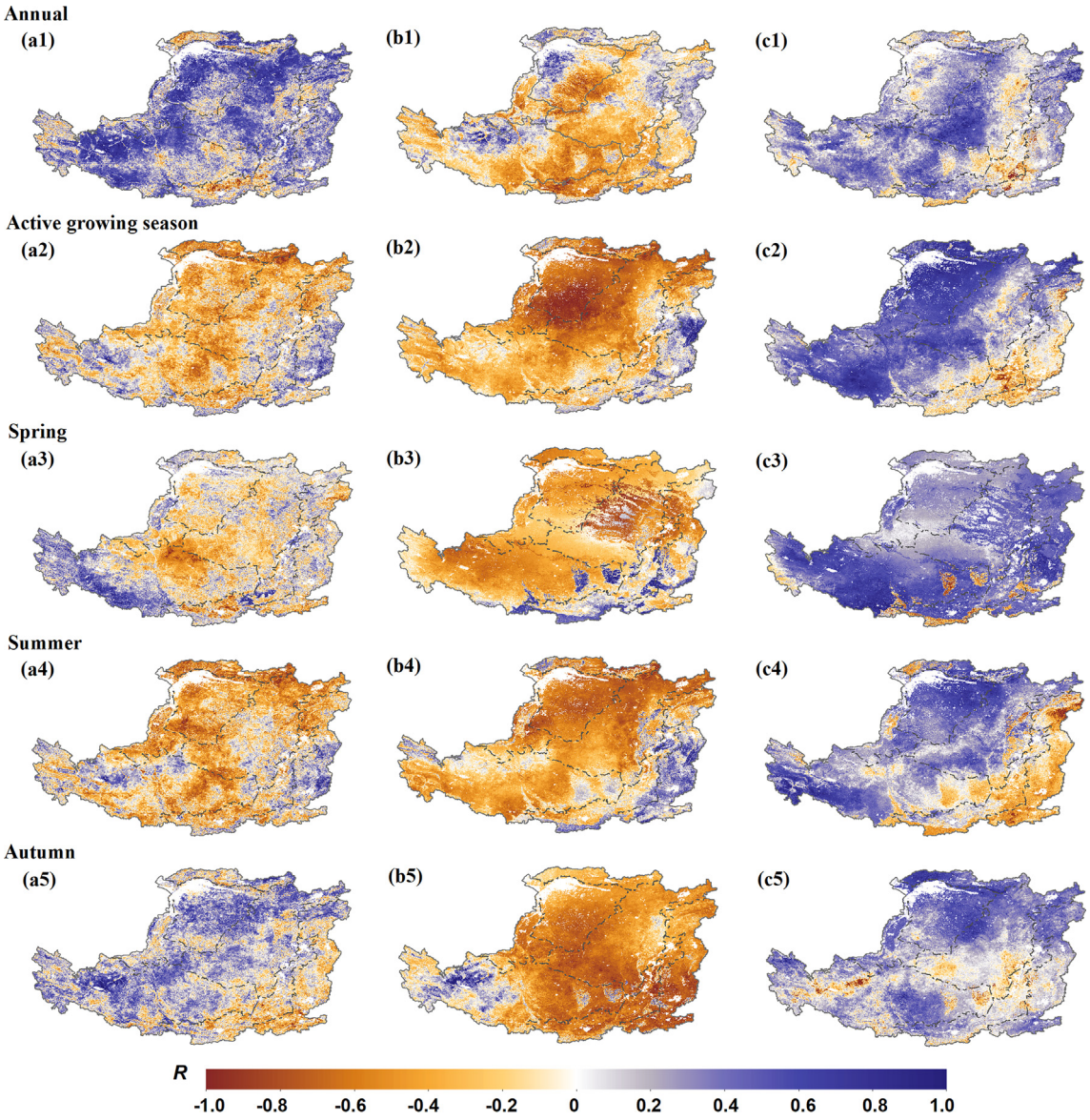

Fig. 6. Spatial patterns of correlation coefficients between detrended series of (a) NDVI, (b) precipitation (P), (c) air temperature (T_a) and WUE during 2000–2014 at the timeframes of (1) annual, (2) active growing season, (3) spring, (4) summer, and (5) autumn in the CLP.

Although the annual WUE trends varied regionally, positive WUE trends were observed in the majority of CLP areas (significantly increased over 68.9% of the entire region, Table 1). As the annual T_a decreased over most CLP areas, the T_a-induced annual WUE should decrease considering the negative feedbacks between ET and T_a discussed above. Concerning the negative response of changes in WUE to P, annual WUE is expected to decrease as well with generally non-significant increasing annual P (Fig. S3b1). Thus, the effects of T_a and P changes during 2000–2014 were decreasing annual WUE in the CLP. Therefore, the enhanced annual WUE in the CLP was determined by the positive response of WUE trends to the increasing vegetation coverage (i.e., higher NDVI). Previous studies have manifested revegetation under the GFG project as the main reason for the remarkable improvement of vegetation coverage in the CLP for the last decade (e.g., Chen et al., 2015; Lü et al., 2012), which indicate that revegetation-induced vegetation coverage change rather than P and T_a changes was the dominant factor driving the increase of annual WUE during 2000–2014 in the CLP.

Although the positive correlations between summer NDVI and summer GPP were consistently stronger as compared to ET as expected (Panels a4 in Figs. 7 and 8), faster increase of ET than that of GPP was observed over 45.8% of the CLP area with significant changes in summer WUE, leading to decreasing summer WUE for these areas (i.e., pixels of 'WUE-GPP + ET+' in Fig. 3b4). The major reason for this is that, the increase of ET stimulated by increasing P was much faster than that of GPP under relatively high temperatures during summers particularly in the southwestern CLP areas (Panels b4 in Figs. 7 and 8). And it has offset the differences between the changes of GPP and ET caused by increasing NDVI. Similar patterns occurred for spring WUE in the southwestern CLP (~17% of the CLP area, Fig. 3a3 and b3) and also AGS WUE because of the vital role of summer in AGS (Fig. 3a2 and b2). Our findings also suggested that the spatial distribution of annual WUE trends were mostly similar with that of autumn WUE trends (Fig. 3a1 and a5). However, unlike the annual WUE trends, the majority of positive autumn WUE trends (~75% of entire CLP area) were caused by decreasing autumn ET (i.e., pixels of 'WUE + GPP + ET-' in Fig. 3b5). It is contributed by the decreasing soil evaporation when NDVI increased. These results suggest that the asymmetric effects of vegetation coverage and climate changes on GPP and ET trends varied for different seasons, hence leading to the varying WUE trends.

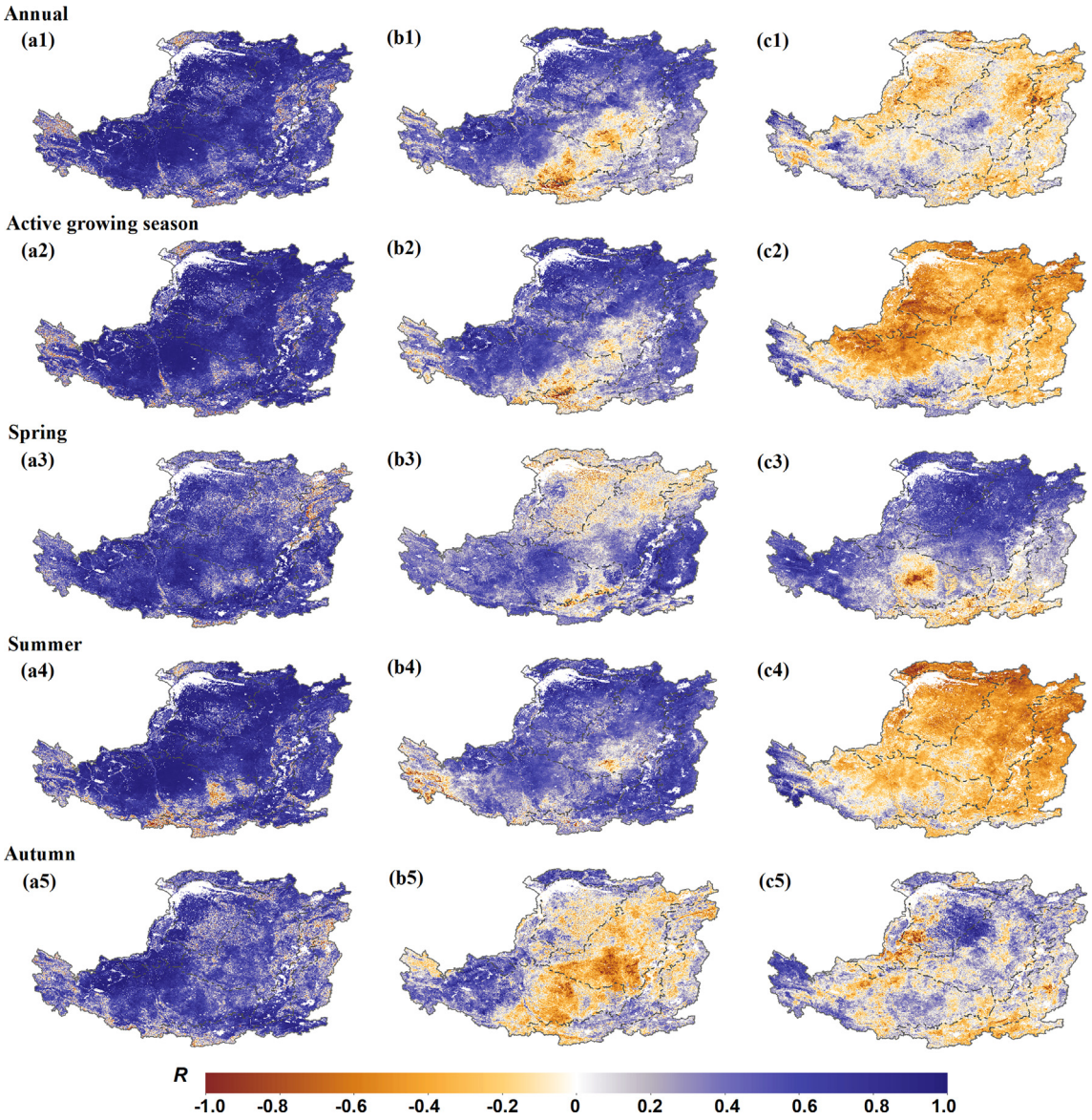

Fig. 7. Spatial patterns of correlation coefficients (R) between GPP and (a) NDVI, (b) P, and (c) T_a during 2000–2014 at the timeframes of (1) annual, (2) active growing season, (3) spring, (4) summer and (5) autumn in the CLP.

It should be noted that GPP is not the 'net' productivity from plant photosynthesis because approximate half of annual GPP are consumed by plant autotrophic respiration, while the residual part of GPP (i.e., NPP) is generally regarded as the material basis for aboveground and belowground biomass in plant communities (Chapin et al., 2006; Wang et al., 2015). To investigate the conclusions obtained above, annual NPP was also utilized to calculate ecosystem WUE (i.e., WUE_{NPP} = NPP/ET). It turned out that WUE_{NPP} significantly increased over 58.4% of the entire CLP area, and correlated with IAV of NDVI, P and T_a in the same manner as that of GPP-derived WUE (Figs. S7–S8). Therefore, our findings based on remote-sensing datasets could strongly support that ecosystem annual WUE has substantially increased in the CLP during 2000–2014, and the vegetation coverage increases rather than P and T_a changes was the primary cause driving the temporal variations in annual WUE in the CLP.

4.4. Uncertainties and future improvements

This study was mainly based on MODIS GPP/NPP and ET data products. The MODIS GPP and ET data were validated with limited sites, so some uncertainties could be caused in the WUE analyses due to the uncertainties from the algorithms and inputs of MODIS GPP/NPP and ET datasets. For example, the biome type information in the MODIS GPP/NPP and ET algorithms is derived from the MODIS MOD12Q1 data product (Friedl et al., 2002). Thus, misclassified land cover from MOD12Q1 could cause less reliable GPP/NPP and ET data. The global 1-km^2 land cover classification from MOD12Q1 may be too coarse for the local heterogeneous landforms in the CLP. Also, the land use/cover changes have not been considered in MOD12Q1, which will bring large uncertainties for GPP/NPP and ET data and hence WUE data for some regions in the CLP. Uncertainties in the global meteorological datasets used in the MODIS GPP/NPP and ET algorithms could also cause some uncertainties for the GPP/NPP and ET estimates. Therefore, it is necessary to improve the accuracy of land cover products and meteorological datasets, which will certainly reduce uncertainties in the GPP/NPP and ET simulations and hence WUE analyses in the CLP.

5. Conclusion

The spatial and temporal variations in the CLP ecosystem water-use

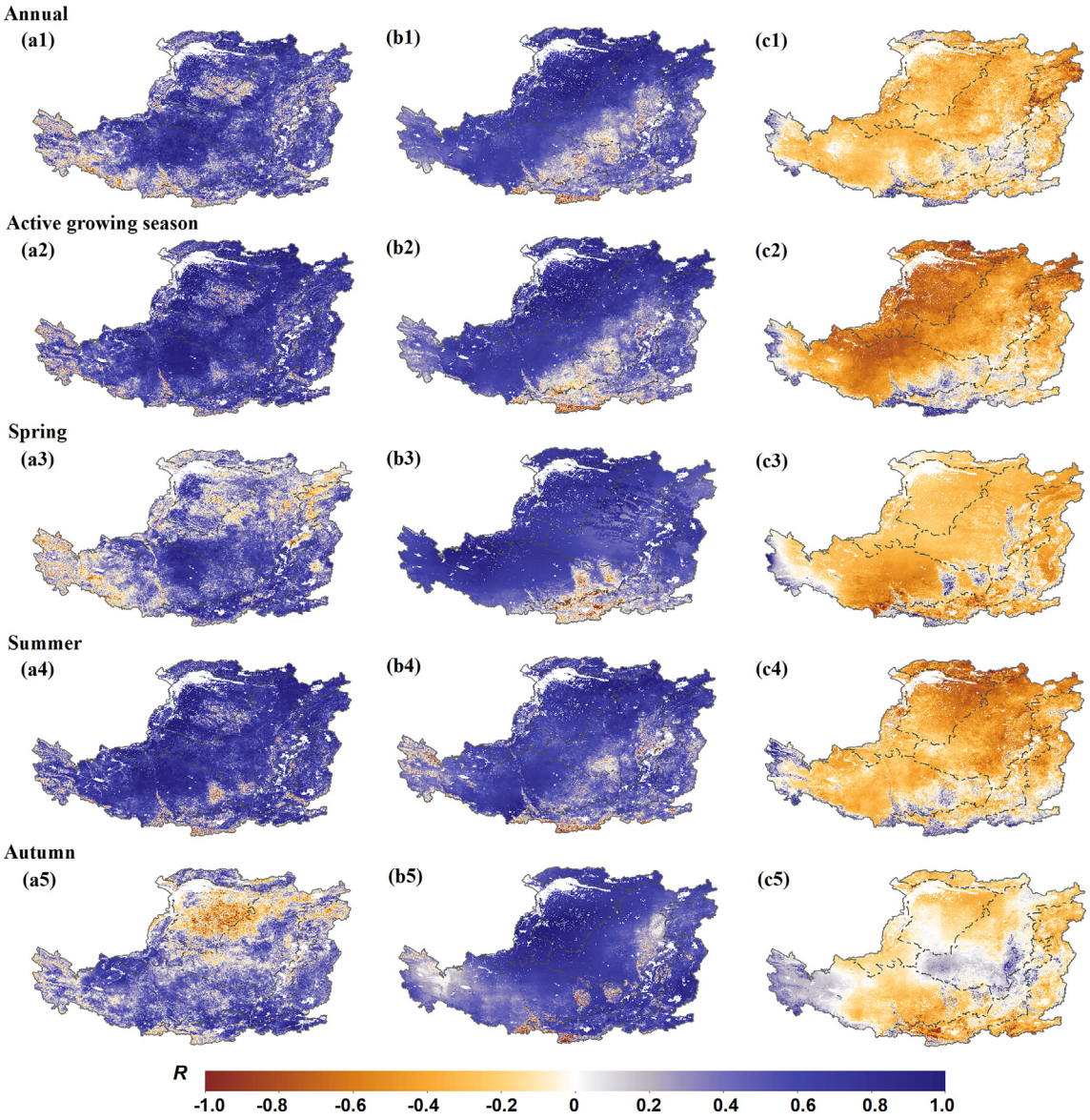

Fig. 8. Spatial patterns of correlation coefficients (R) between ET and (a) NDVI, (b) P, and (c) T_a during 2000–2014 at the timeframes of (1) annual, (2) active growing season, (3) spring, (4) summer and (5) autumn in the CLP.

efficiency (WUE) were analyzed to investigate the responses of WUE variation to regional climate and vegetation coverage changes using MODIS GPP/NPP and ET datasets from 2000 to 2014. Our results demonstrate the spatial patterns of annual WUE and active growing season (AGS) WUE being distinctly different in the CLP, with generally higher annual WUE but lower AGS-WUE for the semi-humid southeastern CLP areas. Significant increases were observed in the annual and autumn WUE at both the per-pixel and spatial-average levels, while WUE for the AGS and different seasons remained stable over most areas in the CLP. Detrended correlation analyses showed that WUE trends were positively correlated with NDVI and air temperature (T_a) variations, and negatively correlated with precipitation (P) variation during 2000–2014 in most situations. Our results suggest that revegetation-induced increase in vegetation coverage rather than P and T_a changes was the primary cause that drove the temporal variations in annual WUE in the CLP. Our findings are important for understanding the revegetation effects on the tradeoffs between ecosystem water and carbon cycles.

Acknowledgements

This work was financially supported by National Natural Science Foundation of China (No. 31700414, 31500390, 41790444), National Key Research and Development Program of China (No. 2016YFA0600104, 2016YFA0600103), and Science and Technology Service Network Initiative of the Chinese Academy of Sciences (No. KFJ-SW-STS-169). We acknowledge the database and technical support from China Meteorological Data Service Center, Numerical Terra Dynamic Simulation Group, and the LAADS DAAC of the NASA in the USA. We thank the editors and anonymous reviewers for their constructive comments that helped improve the quality of this paper.

Appendix A. Supplementary data

Supplementary data to this article can be found online at https://doi.org/10.1016/j.ecolind.2019.02.049.

References

Beer, C., Ciais, P., Reichstein, M., Baldocchi, D., Law, B.E., Papale, D., Soussana, J.F., Ammann, C., Buchmann, N., Frank, D., 2009. Temporal and among-site variability of inherent water use efficiency at the ecosystem level. Global Biogeochem. Cy. 23, GB2018.

Chapin, F.S., Woodwell, G.M., Randerson, J.T., Rastetter, E.B., Lovett, G.M., Baldocchi, D.D., Clark, D.A., Harmon, M.E., Schimel, D.S., Valentini, R., 2006. Reconciling carbon-cycle concepts, terminology, and methods. Ecosystems 9, 1041–1050.

Chen, Y., Wang, K., Lin, Y., Shi, W., Song, Y., He, X., 2015. Balancing green and grain trade. Nat. Geosci. 8, 739–741.

Cowan, I., 1978. Stomatal behaviour and environment. Adv. Botanical Res. 4, 117–228.

Editorial Committee of Vegetation Map of China (ECVMC), 2007. Vegetation map of the People's Republic of China (1:1000000). Geology Publishing House, Beijing, China.

Farquhar, G.D., Sharkey, T.D., 1982. Stomatal conductance and photosynthesis. Ann. Rev. Plant Physiol. 33, 317–345.

Feng, X., Fu, B., Piao, S., Wang, S., Ciais, P., Zeng, Z., Lü, Y., Zeng, Y., Li, Y., Jiang, X., Wu, B., 2016. Revegetation in China's Loess Plateau is approaching sustainable water resource limits. Nat. Climate Change 6, 1019–1022.

Feng, X.M., Sun, G., Fu, B.J., Su, C.H., Liu, Y., Lamparski, H., 2012. Regional effects of vegetation restoration on water yield across the Loess Plateau, China. Hydrol. Earth Syst. Sci. 16, 2617–2628.

Friedl, M.A., Mciver, D.K., Hodges, J.C.F., Zhang, X.Y., Muchoney, D., Strahler, A.H., Woodcock, C.E., Gopal, S., Schneider, A., Cooper, A., 2002. Global land cover mapping from MODIS: algorithms and early results. Remote Sens. Environ. 83, 287–302.

Fu, B., Wang, S., Liu, Y., Liu, J., Liang, W., Miao, C., 2017. Hydrogeomorphic ecosystem responses to natural and anthropogenic changes in the loess plateau of China. Ann. Rev. Earth Planetary Sci. 45, 223–243.

Gao, Y., Zhu, X., Yu, G., He, N., Wang, Q., Tian, J., 2014a. Water use efficiency threshold for terrestrial ecosystem carbon sequestration in China under afforestation. Agric. Forest Meteorol. 195–196, 32–37.

Gao, Y.N., Yu, G.R., Yan, H.M., Zhu, X.J., Li, S.G., Wang, Q.F., Zhang, J.H., Wang, Y.F., Li, Y.N., Zhao, L., Shi, P.L., 2014b. A MODIS-based photosynthetic capacity model to estimate gross primary production in Northern China and the Tibetan Plateau. Remote Sens. Environ. 148, 108–118.

Hu, Z., Yu, G., Fu, Y., Sun, X., Li, Y., Shi, P., Wang, Y., Zheng, Z., 2008. Effects of vegetation control on ecosystem water use efficiency within and among four grassland ecosystems in China. Global Change Biol. 14, 1609–1619.

Huang, L., He, B., Han, L., Liu, J., Wang, H., Chen, Z., 2017. A global examination of the response of ecosystem water-use efficiency to drought based on MODIS data. Sci. Total Environ. S601–602, 1097–1107.

Huang, M., Piao, S., Sun, Y., Ciais, P., Cheng, L., Mao, J., Poulter, B., Shi, X., Zeng, Z., Wang, Y., 2015. Change in terrestrial ecosystem water-use efficiency over the last three decades. Glob Chang Biol. 21, 2366–2378.

Hutchinson, M., 1995. Interpolating mean rainfall using thin plate smoothing splines. Int. J. Geogr. Inf. Syst. 9, 385–403.

Huxman, T.E., Smith, M.D., Fay, P.A., Knapp, A.K., Shaw, M.R., Loik, M.E., Smith, S.D., Tissue, D.T., Zak, J.C., Weltzin, J.F., 2004. Convergence across biomes to a common rain-use efficiency. Nature 429, 651.

Jasechko, S., Sharp, Z.D., Gibson, J.J., Birks, S.J., Yi, Y., Fawcett, P.J., 2013. Terrestrial water fluxes dominated by transpiration. Nature.

Jung, M., Reichstein, M., Margolis, H.A., Cescatti, A., Richardson, A.D., Arain, M.A., Arneth, A., Bernhofer, C., Bonal, D., Chen, J., Gianelle, D., Gobron, N., Kiely, G., Kutsch, W., Lasslop, G., Law, B.E., Lindroth, A., Merbold, L., Montagnani, L., Moors, E.J., Papale, D., Sottocornola, M., Vaccari, F., Williams, C., 2011. Global patterns of land-atmosphere fluxes of carbon dioxide, latent heat, and sensible heat derived from eddy covariance, satellite, and meteorological observations. J. Geophys. Res. 116, G00J07.

Keenan, T.F., Hollinger, D.Y., Bohrer, G., Dragoni, D., Munger, J.W., Schmid, H.P., Richardson, A.D., 2013. Increase in forest water-use efficiency as atmospheric carbon dioxide concentrations rise. Nature 499, 324.

Khalifa, M., Elagib, N.A., Ribbe, L., Schneider, K., 2018. Spatio-temporal variations in climate, primary productivity and efficiency of water and carbon use of the land cover types in Sudan and Ethiopia. Sci. Total Environ. 624, 790–806.

Law, B., Falge, E., Gu, L., Baldocchi, D., Bakwin, P., Berbigier, P., Davis, K., Dolman, A., Falk, M., Fuentes, J., 2002. Environmental controls over carbon dioxide and water vapor exchange of terrestrial vegetation. Agric. Forest Meteorol. 113, 97–120.

Li, S., Liang, W., Fu, B., Lü, Y., Fu, S., Wang, S., Su, H., 2016. Vegetation changes in recent large-scale ecological restoration projects and subsequent impact on water resources in China's Loess Plateau. Sci. Total Environ. S569–570, 1032–1039.

Li, W., Liu, Y.J., Yang, Z., 2012. Preliminary strategic environmental assessment of the Great Western Development Strategy: safeguarding ecological security for a new western China. Environ. Manage. 49, 483.

Liu, D., An, Z., Wen, Q., Lu, Y., Han, J., Wang, J., Diao, G., 1978. Geological environment of Chinese Loess. Chinese Sci. Bullet 1-9 + 26.

Liu, D., Chen, Y., Cai, W., Dong, W., Xiao, J., Chen, J., Zhang, H., Xia, J., Yuan, W., 2014. The contribution of China's Grain to Green Program to carbon sequestration. Landscape Ecol. 29, 1675–1688.

Liu, W., 2015. Scientific understanding of the Belt and Road Initiative of China and related research themes. Progr. Geogr. 34, 538–544.

Lü, H., Liu, D., Guo, Z., 2003. Natural vegetation of geological and historical periods in Loess Plateau. Chin Sci. Bullet. 48, 411–416.

Lü, Y., Fu, B., Feng, X., Zeng, Y., Liu, Y., Chang, R., Sun, G., Wu, B., 2012. A policy-driven large scale ecological restoration: quantifying ecosystem services changes in the Loess Plateau of China. PLoS One 7, e31782.

McVicar, T.R., Li, L., Van Niel, T.G., Zhang, L., Li, R., Yang, Q., Zhang, X., Mu, X., Wen, Z., Liu, W., Zhao, Y.A., Liu, Z., Gao, P., 2007. Developing a decision support tool for China's re-vegetation program: simulating regional impacts of afforestation on average annual streamflow in the Loess Plateau. Forest Ecol. Manage. 251, 65–81.

Mu, Q., Heinsch, F.A., Zhao, M., Running, S.W., 2007. Development of a global evapotranspiration algorithm based on MODIS and global meteorology data. Remote Sens. Environ. 111, 519–536.

Mu, Q., Zhao, M., Running, S.W., 2011. Improvements to a MODIS global terrestrial evapotranspiration algorithm. Remote Sens. Environ. 115, 1781–1800.

National Development and Reform Commission (NDRC), 2010. Comprehensive management planning outline of China's loess plateau (2010-2030). Ministry of Water Resources, Ministry of Agriculture, State Forestry Administration, Central People's Government of the People's Republic of China, http://www.gov.cn/zwgk/2011-01/17/ content_1786454.htm (in Chinese).

Nemani, R.R., Keeling, C.D., Hashimoto, H., Jolly, W.M., Piper, S.C., Tucker, C.J., Myneni, R.B., Running, S.W., 2003. Climate-driven increases in global terrestrial net primary production from 1982 to 1999. Science 300, 1560–1563.

Niu, S.L., Xing, X.R., Zhang, Z., Xia, J.Y., Zhou, X.H., Song, B., Li, L.H., Wan, S.Q., 2011. Water-use efficiency in response to climate change: from leaf to ecosystem in a temperate steppe. Global Change Biol. 17, 1073–1082.

Piao, S., Friedlingstein, P., Ciais, P., de Noblet-Ducoudre, N., Labat, D., Zaehle, S., 2007. Changes in climate and land use have a larger direct impact than rising CO2 on global river runoff trends. Proc. Natl. Acad. Sci. USA 104, 15242–15247.

Running, S.W., Nemani, R.R., Heinsch, F.A., Zhao, M., Reeves, M., Hashimoto, H., 2004. A continuous satellite-derived measure of global terrestrial primary production. Bioscience 54, 547–560.

Su, C., Fu, B., 2013. Evolution of ecosystem services in the Chinese Loess Plateau under climatic and land use changes. Global Planetary Change 101, 119–128.

Sun, Y., Piao, S., Huang, M., Ciais, P., Zeng, Z., Cheng, L., Li, X., Zhang, X., Mao, J., Peng, S., Poulter, B., Shi, X., Wang, X., Wang, Y.-P., Zeng, H., 2016. Global patterns and climate drivers of water-use efficiency in terrestrial ecosystems deduced from satellite-based datasets and carbon cycle models. Global Ecol. Biogeogr. 25, 311–323.

Wang, K.C., Dickinson, R.E., 2012. A review of global terrestrial evapotranspiration: observation, modeling, climatology, and climatic variability. Rev. Geophys. 50, RG2005.

Wang, Q., Zheng, H., Zhu, X., Yu, G., 2015. Primary estimation of Chinese terrestrial carbon sequestration during 2001–2010. Sci. Bullet. 60, 577–590.

Xiao, J., 2014. Satellite evidence for significant biophysical consequences of the "Grain for Green" Program on the Loess Plateau in China. J. Geophys. Res.: Biogeosci. 119, 2261–2275.

Xiao, J., Sun, G., Chen, J., Chen, H., Chen, S., Dong, G., Gao, S., Guo, H., Guo, J., Han, S., 2013. Carbon fluxes, evapotranspiration, and water use efficiency of terrestrial ecosystems in China. Agric. Forest Meteorol. 182, 76–90.

Yao, Y., Liang, S., Cheng, J., Liu, S., Fisher, J.B., Zhang, X., Jia, K., Zhao, X., Qin, Q., Zhao, B., Han, S., Zhou, G., Zhou, G., Li, Y., Zhao, S., 2013. MODIS-driven estimation of terrestrial latent heat flux in China based on a modified Priestley-Taylor algorithm. Agric. Forest Meteorol. 171–172, 187–202.

Yu, L., Kang, R., Mulder, J., Zhu, J., Dörsch, P., 2017. Distinct fates of atmogenic NH_4^+ and NO_3^- in subtropical, N-saturated forest soils. Biogeochemistry 133, 279–294.

Yu, G., Song, X., Wang, Q., Liu, Y., Guan, D., Yan, J., Sun, X., Zhang, L., Wen, X., 2008. Water-use efficiency of forest ecosystems in eastern China and its relations to climatic variables. New Phytologist 177, 927–937.

Yu, G.R., Wang, Q.F., Zhuang, J., 2004. Modeling the water use efficiency of soybean and maize plants under environmental stresses: application of a synthetic model of photosynthesis-transpiration based on stomatal behavior. J. Plant Physiol. 161, 303–318.

Zeng, Z., Wang, T., Zhou, F., Ciais, P., Mao, J., Shi, X., Piao, S., 2014. A worldwide analysis of spatiotemporal changes in water balance-based evapotranspiration from 1982 to 2009. J. Geophys. Res.: Atmospheres 119, 1186–1202.

Zhang, K., Kimball, J.S., Nemani, R.R., Running, S.W., 2010. A continuous satellite-derived global record of land surface evapotranspiration from 1983 to 2006. Water Resour. Res. 46, W09522.

Zhang, T., Peng, J., Liang, W., Yang, Y., Liu, Y., 2016. Spatial-temporal patterns of water use efficiency and climate controls in China's Loess Plateau during 2000–2010. Sci. Total Environ. 565, 105–122.

Zhao, M., Heinsch, F.A., Nemani, R.R., Running, S.W., 2005. Improvements of the MODIS terrestrial gross and net primary production global data set. Remote Sens. Environ. 95, 164–176.

Zheng, H., Yu, G., Wang, Q., Zhu, X., He, H., Wang, Y., Zhang, J., Li, Y., Zhao, L., Zhao, F., 2016. Spatial variation in annual actual evapotranspiration of terrestrial ecosystems in China: results from eddy covariance measurements. J. Geographical Sci. 26, 1391–1411.

Zhu, Q., Jiang, H., Peng, C., Liu, J., Wei, X., Fang, X., Liu, S., Zhou, G., Yu, S., 2011. Evaluating the effects of future climate change and elevated CO 2 on the water use efficiency in terrestrial ecosystems of China. Ecol. Modell. 222, 2414–2429.

Zhu, X.J., Yu, G.R., Wang, Q.F., Hu, Z.M., Zheng, H., Li, S.G., Sun, X.M., Zhang, Y.P., Yan, J.H., Wang, H.M., Zhao, F.H., Zhang, J.H., Shi, P.L., Li, Y.N., Zhao, L., Zhang, F.W., Hao, Y.B., 2015. Spatial variability of water use efficiency in China's terrestrial ecosystems. Global Planet. Change 129, 37–44.

Zhu, Z., Bi, J., Pan, Y., Ganguly, S., Anav, A., Xu, L., Samanta, A., Piao, S., Nemani, R.R., Myneni, R.B., 2013. Global Data Sets of Vegetation Leaf Area Index (LAI)3g and Fraction of Photosynthetically Active Radiation (FPAR)3g Derived from Global Inventory Modeling and Mapping Studies (GIMMS) Normalized Difference Vegetation Index (NDVI3g) for the Period 1981 to 2011. Remote Sens. 5, 927–948.